Microstructural Characterisation of Metals and Alloys

by

P E J FLEWITT and R K WILD

Book 327
published in February 1985 by
The Institute of Metals
1 Carlton House Terrace
London SW1Y 5DB

ISBN 0 904357 76 7

P E J FLEWITT

BSc, PhD, DSc(Lond), FInstP, CEng, MIM, Section Head, Scientific Services Department, Central Electricity Generating Board, South Eastern Region

Following a period of post-doctoral work as University Research Fellow in the Department of Metallurgy at Sheffield University, Peter Flewitt joined, in 1969, the Scientific Services Department of the Central Electricity Generating Board, South Eastern Region, where he currently holds the post of Head of the Integrity of Machines and Structures Section. In 1980 he was awarded the degree of Doctor of Science by London University for work on the relationship between microstructure and the physical properties of materials. He is also a Visiting Reader in the Department of Physics at Surrey University.

R K WILD

BSc, PhD, MInstP, MIM, Research Officer in Technology, Research and Planning Department, Central Electricity Generating Board, Berkeley Nuclear Laboratories

Bob Wild graduated in Physics at Reading University in 1963 where he continued until 1966, gaining a PhD for work on the plastic deformation of diamond. He then held the post of Assistant Professor at the Physics Department of the University of Virginia, Charlottesville, USA, during which time he worked on the plastic properties of copper-aluminium alloys. Returning to England in 1968, he joined the Central Electricity Generating Board, working at Berkeley Nuclear Laboratories where he has developed his current research interests which include the oxidation of nickel-chromium steels and the properties of surfaces and interfaces.

Compiled from master typescript and illustrations prepared by the authors

Printed and made in England by The Chameleon Press Ltd, London

CONTENTS

1 INTRODUCTION

It is the aim of this monograph to provide students of metallurgy, materials science and solid state physics with a guide to those techniques and procedures which enable the microstructure of metals and alloys to be completely characterised. In general pure metals are opaque, lustrous and relatively heavy, are easily fabricated and shaped, have good mechanical strength and high thermal and electrical conductivity. All these properties are a consequence of the metallic bond; metal atoms have only a few electrons in the outer electron shell which are shared between atoms forming an electron cloud and bond by Coulomb attraction. Changes in the strength of this bond cause differences in optical, electrical, mechanical and thermal properties of various metals and alloys (1-3). The simple, regular crystalline structures of metals result from this non-specific and non-directional bond which holds atoms in close packed arrangements so that the pure metals, generally, have one of the face centred cubic (fcc), body centred cubic (bcc) or hexagonal close packed (hcp) structures of the fourteen crystal systems, Figure 1.1. These crystallographic arrangements give rise to materials of relatively high ductility since they are resistant to tensile stresses and less resistant to shearing forces. However, the overall mechanical properties of metals are controlled by the 'defect' structure within the crystallographic arrangement of atoms such as dislocations, point defects, etc (4-6). Mechanical and chemical properties can be modified by the addition of alloying elements which are used to advantage in a range of commercial materials. In many alloy systems compositions and heat treatments are selected that produce complex distributions of phases to give the required properties (7). To understand the response of metals and alloys to static, dynamic and cyclic stresses, various environments and temperatures, it is essential to be able to describe the 'total microstructure'. For this it may be necessary to combine a knowledge of the chemical composition, crystal and defect structure, and the proportion and distribution of various phases present.

The fundamentals of microstructural investigations of metals and alloys were laid over a hundred years ago by Henry Clifford Sorby who developed a preparation method and etching treatment for viewing metal samples under a reflected light microscope (8). Indeed it is this technique, progressively refined, which remains a powerful tool to the metallographer for establishing essential microstructural features such as grain size and shape and distributions of phases to the limit of resolution of the optical microscope ~ 300nm. The development in the early 1950's of a theoretical understanding of the principles controlling the strength of materials resulted in a need to consider techniques with resolutions approaching that of an interatomic spacing. This led to the use of electrons where the shorter wavelengths enable resolutions of ~ 0.2nm to be achieved with current generation electron microscopes. The electron microscope, developed in 1931, was initially used to study biological systems (9) but techniques for sample replication and the preparation of thin metal foils in the mid-1950's enabled microstructural investigations to be undertaken on metals and alloys (9-11). Since then the resolution has been improved and the accelerating voltages increased (12)(13). An area of advance has been to extend the atomic, structural and crystallographic information obtained by X-ray diffraction techniques to the small-scale features contained within thin foil samples using methods based on electron diffraction. Over the last decade attention has focussed on establishing chemical information within a microstructure to a very high spatial resolution. Certainly in the early 1960's the introduction of the electron probe microanalyser enabled relatively high spatial resolution

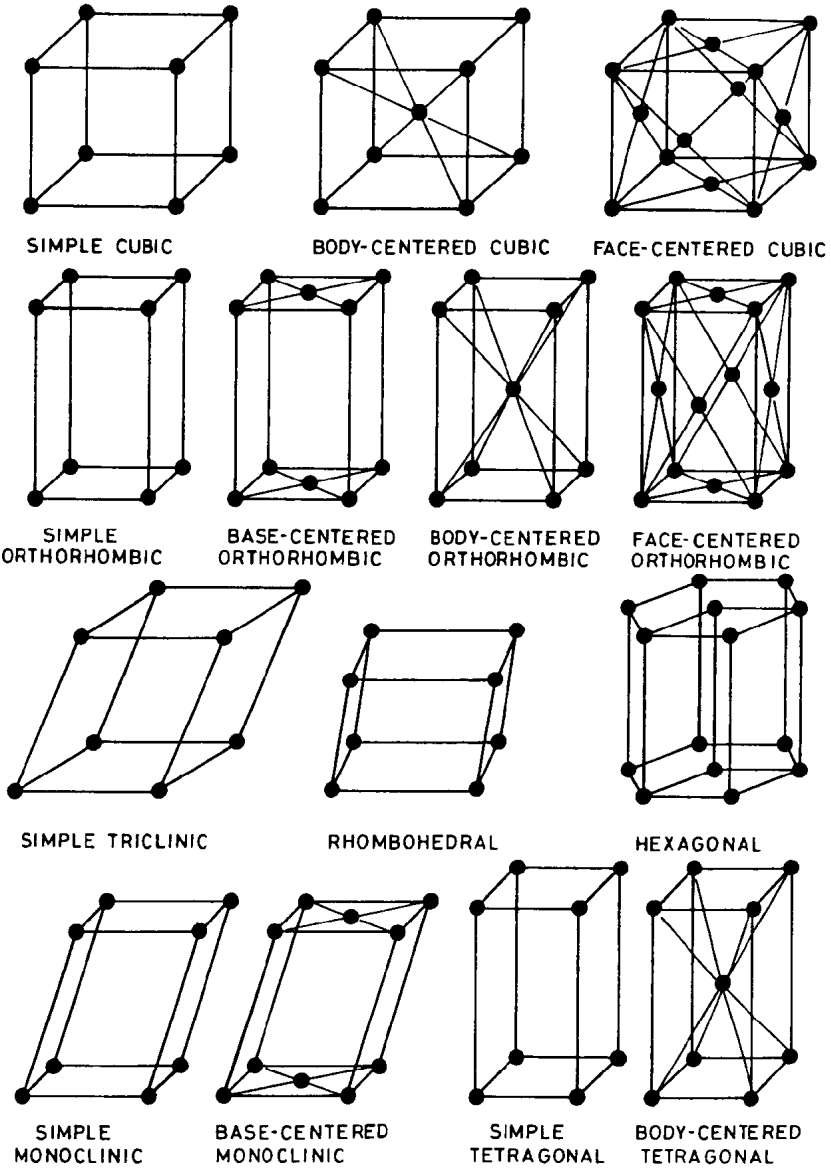

Figure 1.1 The fourteen crystal systems for all crystalline solids. Generally pure metals adopt either the body centred cubic (bcc), face centred cubic (fcc) or hexagonal close packed (hcp) close packing arrangements.

chemical analyses, using characteristic X-ray emissions, to be obtained from features down to ~ 1μm diameter. However, since that time it has become evident that chemical changes over distances approaching atomic dimensions have a profound effect on mechanical and chemical properties of metals and alloys (14)(15). For example, the segregation of trace impurities to grain boundaries in polycrystalline materials to give single atom layer coverage can drastically modify the properties of an alloy. To study these segregations a number of techniques have been developed with a good depth resolution for surface analysis such as X-ray photoelectron spectroscopy, Auger electron spectroscopy and secondary ion mass spectrometry which together with the high spatial resolution techniques of scanning and transmission electron microscopy used in conjunction with energy dispersive X-ray and electron energy loss spectroscopy have further improved the state of knowledge in this area.

It is an appropriate time to appraise these developments and to review techniques which permit the complete characterisation of the microstructure within a metal or alloy. Certainly techniques are reaching a stage where potentially it is possible to establish the information necessary to correlate existing theoretical models describing high and low temperature deformation and fracture, corrosion, oxidation, environmentally assisted fracture, electrical and other physical properties with the material microstructure. It is the intention of this monograph to consider briefly the theory behind, the relative benefits of, and the application of techniques which have now reached a stage where they are widely available as a tool for use by research scientists although not necessarily considered to be suitable for routine application. As a consequence certain basic techniques are assumed and less attention given to optical microscopy although this is not intended to imply that this is not a powerful and essential technique for many microstructural evaluations. Indeed, with the advent of computer based image analysis and pattern recognition techniques (16-18), optical methods with their advantages of simplicity and low cost may be further advanced in the quantitative evaluation of certain microstructural parameters. Finally, examples of particular problems are considered to provide a guide to the interactive use of techniques, to derive that information which enables an improved understanding of the role that microstructure has on controlling a particular physical property of a metal or alloy.

REFERENCES

(1) A.H. Cottrell, An Introduction to Metallurgy, Edward Arnold (London) 1967.
(2) N.F. Mott and H. Jones, The Theory of the Properties of Metals and Alloys, Dover, (New York), 1958.
(3) N.F. Mott, The Solid State, Scientific American 1976, p.80.
(4) F.R.N. Nabarro, Theory of Crystal Dislocations, Clarendon Press (Oxford) 1967.
(5) W. Bollman, Crystal Defects and Crystalline Interfaces, Springer (Berlin) 1970.
(6) R.W.K. Honeycombe, The Plastic Deformation of Metals, Edward Arnold (London) 1968.
(7) C.S. Barrett and T.B. Massalski, Structure of Metals, McGraw-Hill (Third edition) (New York) 1966.
(8) A.G. Quarrell, 15th Hatfield Memorial Lecture, 'Metallography', I.S.I Special Report No. 80, Eyre and Spottiswoode (London) 1963, p.1.
(9) E. Ruska, Fifth Int. Congress for Electron Microscopy; Philadelphia 1962, ed. S.S. Bleese, Academic Press (London) 1962.

(10) P.B. Hirsch, Proceedings of the Third International Conference on Electron Microscopy, (London) 1954, 231.
(11) G. Thomas, Transmission Electron Microscopy of Metals, Wiley and Sons, (New York) 1962.
(12) M. Isaacson, M. Ohtsuki and M. Utlaut, Electron Microscopy of Individual Atoms, in 'Introduction to Analytical Electron Microscopy', ed. J.J. Hren, J.I. Goldstein and D.C. Joy, Plenum Press (New York), 1979.
(13) B.Jouffrey, Electron Microscopy in Materials Science, Part III, Ed. E. Ruedl and U. Valdré, Commission of European Communities (Brussels) 1976, p.981.
(14) E.D. Hondros and M.P. Seah, Met. Rev., 1977 22 262.
(15) C.J. McMahon, Mat. Sci. and Eng., 1980, 42 215.
(16) D. Bruggins, Optical and Electron Microscopy, 1983, Issue 3, 9.
(17) W.O. Saxton, Computer Techniques for Image Processing, in 'Electron Microscopy', Academic Press (New York) 1978.
(18) R.W. Horne and R. Markham, Application of Optical Microscopy in 'Practical Methods in Electron Microscopy', Ed. A.M. Glauert, North-Holland (Amsterdam) 1973, 327.

2 INTERACTION OF ELECTROMAGNETIC RADIATION WITH METALS AND ALLOYS

2.1 Introduction

Since the majority of techniques used to examine the microstructures of metals and alloys depend upon imaging a sample, using either light or electrons and the diffraction of either electrons or X-radiation, it is appropriate to consider some of the concepts and theories on which these techniques are based. We can confine this to a simple guide particularly in the case of electron images and diffraction where three dimensional diffraction processes operate for specimens of useful thickness if optimum resolutions are achieved. Certainly many of the optical concepts apply equally to the electron optical systems.

2.2 Resolution

The ability to resolve detail within a visual image is a basic requirement for microstructural investigations. Essentially resolution defines the smallest separation of two points in the object which may be distinctly reproduced in the image. For a simple, general, optical system, Figure 2.1, applying the Rayleigh criterion to the Abbé formulation (1-3) defines the resolution for light microscopy since this is limited by diffraction of each point within the object which is spread into a small disc in the image (Airy disc). Thus, resolving power, δ, is given by:

$$\delta = k\lambda/n.\sin\alpha \qquad \ldots\ldots 2.1$$

where λ is the wavelength of the illumination, n is the refractive index of the medium between the specimen and the lens, α is the semi-angle subtended by the object at the lens and k is a constant usually taken to be 0.61 depending upon the coherence of the illumination. The quantity $n.\sin\alpha$ defines the numerical aperture of the lens. For an optical microscope with white light illumination ($\lambda \simeq 50$nm) fitted with an oil immersion lens ($n.\sin\alpha = 1.35$) it is possible to achieve a resolution of about 200nm. Resolving power, however, is not the only factor to consider when assessing the performance of an optical microscope. Together with depth of focus it is important that the image should contain sufficient contrast to discriminate against background and this is related to changes in amplitude and absorption characteristics produced by the specimen under incident light as distinct from a change of phase. In the case of electrons the de Broglie relationship (4) relates the wavelength of electrons, λ, to their momentum, mv, (m is mass and v is velocity) by h Planck's constant such that $\lambda = h/mv$. Electrons accelerated by a potential difference of V volts have a kinetic energy of $\frac{1}{2}mv^2$ such that:

$$mv^2 = 2e.V \qquad \ldots\ldots 2.2$$

where e is the electronic charge. Thus:

$$\lambda = h/(2\ m.e.V)^{\frac{1}{2}} \qquad \ldots\ldots 2.3$$

The energy term e.V is expressed in electron volts and represents that energy required to pass an electron through a potential difference of one volt ($1\ eV = 1.602 \times 10^{-19}J$). When the velocity of the electron approaches the speed of light, $v \rightarrow C$, a relativistic correction is required for the voltage such that $V = V\left[1 + eV/2m_o C^2\right]$ where m_o is the mass of an electron at

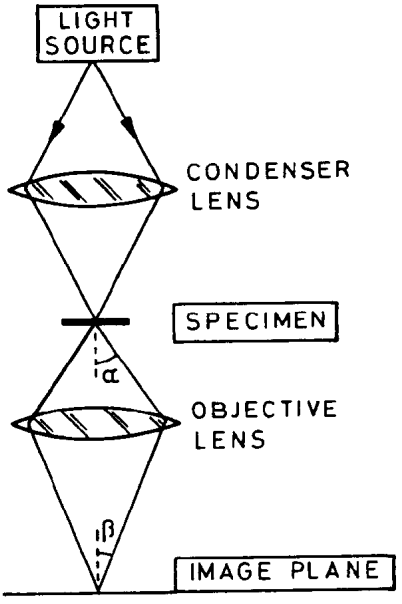

Figure 2.1 A simple optical, transmission microscope system comprising a condenser and objective lens.

Applied Voltage (V) (keV)	Wavelength (λ) (nm)
20	0.008588
50	0.005355
80	0.00418
100	0.003702
200	0.002508
500	0.001421
1000	0.000872

TABLE 2.1 Variation of electron wavelength with applied voltage.

rest. This correction becomes important for $V > 10^5$ volts; at 100 keV it is about 5% which increases to about 30% at 10^6 keV. Wavelengths for accelerating voltages commonly used in electron microscopy are given in Table 2.1 (5).

Many of the current commercial electron microscopes operate with voltages in the range 100 to 300 keV with corresponding electron wavelengths of between 0.004nm and 0.002nm respectively. From equation 2.1 this gives a resolving power of ~ 0.0025nm and ~ 0.0017nm for an efficiently designed electron lens. Spherical aberration is the main factor which limits the performance of electromagnetic lenses used in microscopes and results in α being kept small (in equation 2.1). Indeed resolving power is related to spherical aberration, C_s, by (6):

$$\delta \text{ prop. } \lambda^{\frac{3}{4}} C_s^{\frac{1}{4}} \qquad \ldots\ldots \quad 2.4$$

Therefore, for a transmission instrument operating at 100 keV, with $\lambda \simeq 0.0037$nm and $C_s \simeq 2.337 \times 10^6$ the limit of resolution is $\simeq$ 0.12nm.

2.3 Lens Defects

Lenses used in optical and electron optical systems do not give perfect images because of defects and aberrations (7-10). We will now consider some of these factors.

Spherical Aberration: For paraxial illumination and Gaussian imaging there is a conjugate point to point correspondence between the object and the image. In Figure 2.2(a) the image of the object point X lies in the image plane at Y for all paraxial rays XAY. However, if the rays are not paraxial ($\sin \alpha \neq \alpha$) they are bent more at the periphery of the lens and as such the image point Y is displaced by a distance Δr to Y'. Point Y now has an apparent radius $\Delta r/M$ where M is the image magnification and the image is subject to spherical aberration which is defined by the coefficient, C_s.

Astigmatism: If a lens does not have perfect axial symmetry then the image plane for objects lying in one direction differs from the image plane for objects lying in another direction. Consequently, vertical components of the image focus in a different plane compared to the horizontal components and no sharp image plane exists, only a plane of least confusion between two sharply focussed images. In the case of electron optical instruments stigmators are used to compensate for this particular lens imperfection.

Distortion: Spherical aberration in a lens results in the image magnification varying in proportion to the $(\text{distance})^3$; a point image displaced from the optical axis produces a distorted image, Figure 2.2(b). Pin cushion distortion occurs when the magnification of the image increases with distance of the image point from the centre. The opposite to this is barrel distortion. Spiral distortion arises from the angular rotation of an image point which depends upon the distance of that point from the optical axis and, as a consequence, images assume a sigmoidal shape.

Chromatic Aberration: As a consequence of refraction by either a glass lens or an electromagnetic lens either light or electrons respectively emitted from the source X in Figure 2.2(c) with different wavelengths or velocities, equation 2.2, focus at different points Y and Y'; the greater the velocity or the longer the wavelength the greater the focal length. As a result point X

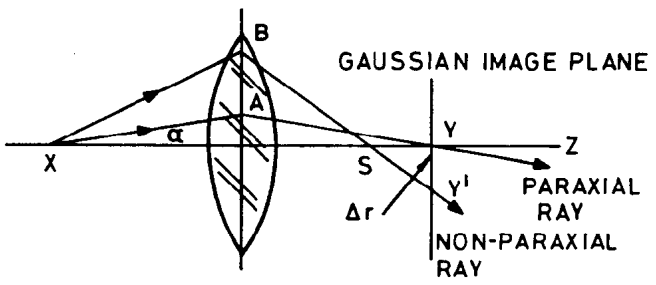

(a)

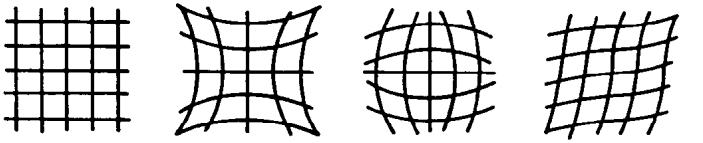

(b)

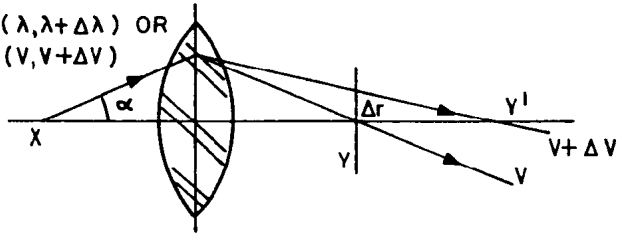

(c)

Figure 2.2 Lens defects:

(a) Paraxial ray X A Y and non-paraxial ray X B Y illlustrating spherical aberration in the image plane.

(b) Commonly encountered distortions in either an optical or electromagnetic lens.

(c) Rays leaving a point X with either different velocities due to potentials V and V + ΔV (electrons), or different wavelengths λ and λ + Δλ (light) will be brought to a focus at Y and Y', respectively; chromatic aberration.

will be imaged as a disc of radius $\Delta r/M$ and this is called chromatic aberration:

$$\Delta r = C_c \alpha (\Delta V/V) \quad \ldots\ldots 2.5$$

where C_c is the chromatic aberration coefficient and $\Delta V/V$ is proportional to $\Delta\lambda/\lambda$.

2.4 Diffraction

X-rays are electromagnetic radiation with wavelengths ~ 0.1nm and as shown by equation 2.2 electrons have similar wave properties. Therefore, when either X-rays or electrons interact with a crystalline material they are subject to diffraction which, for monochromatic radiation, produces a series of strongly diffracted beams leaving the crystal in defined and predicted directions. The relationship between the crystal lattice, the incident radiation and the resultant diffraction pattern is given by Braggs Law (11):

$$n \lambda = 2 d \sin \theta \quad \ldots\ldots 2.6$$

where λ is the wavelength of the incident radiation, d is the spacing between specific crystal planes which make an angle θ with the incident radiation and n is an integer. For commonly encountered diffraction problems use is made of the reciprocal lattice (12) in which sets of lattice planes are represented simply by a set of points in reciprocal space. The reciprocal lattice is constructed for a defined crystal lattice (a unit cell shown in Figure 1.1), by drawing a line from the origin normal to the lattice plane, h,k,l under consideration. This will be of length d^*_{hkl} which is equal to the reciprocal of the interplanar spacing d_{hkl}. The construction of part of a reciprocal lattice for a face centred cubic crystal lattice is shown in Figure 2.3. Here the reciprocal lattice points correspond to both lattice planes with defined Miller indices (h,k,l) and fictitious planes (nh, nk, nl) which may also produce diffraction. Consequently, the reciprocal lattice describes a range of potential diffraction sites for a given crystal lattice. A particular lattice type may be characterised by 'absent' diffraction positions and the corresponding spots within the reciprocal lattice will be missing, for example an fcc Bravais lattice is equivalent to a bcc reciprocal lattice and vice versa.

A geometrical construction within the reciprocal lattice is used to determine the condition for Bragg diffraction. This is illustrated in Figure 2.4 where the incident beam of either X-rays or electrons of wavelength λ is at the origin of the reciprocal lattice. A sphere of radius λ^{-1} is drawn through the origin and diffraction occurs from planes which are intersected by the sphere. Thus, the diffracting planes d_{hkl} have a reciprocal point at r^*_{hkl} which lies on the surface of the sphere of radius λ^{-1} (Ewald sphere) so that equation 2.6 is satisfied if:

$$\underline{g} = \underline{k}_1 - \underline{k}_0 \quad \ldots\ldots 2.7$$

where $\underline{g}$ is the reciprocal lattice vector corresponding to the diffracting planes, $\underline{k}_0$ is the incident wave vector equal to λ^{-1} and $\underline{k}_1$ is the diffracted wave vector. If the diffracting sphere is rotated while touching the reciprocal lattice it sweeps out a limiting sphere of radius $2\lambda^{-1}$ so that all diffracting crystal lattice planes have points lying within the limiting sphere.

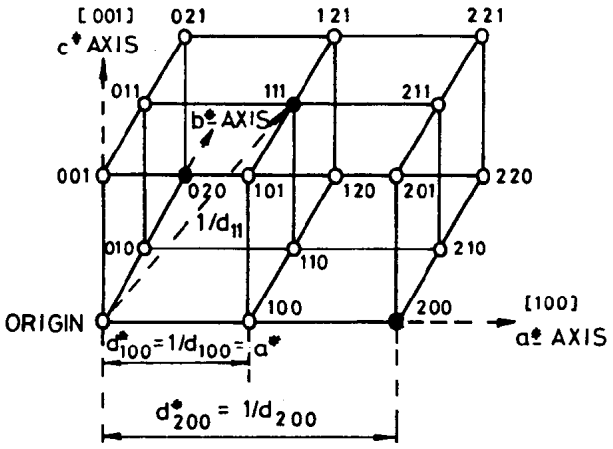

Figure 2.3 The reciprocal lattice for a face centred cubic (fcc) crystal structure; closed circles represent those points which result in diffraction.

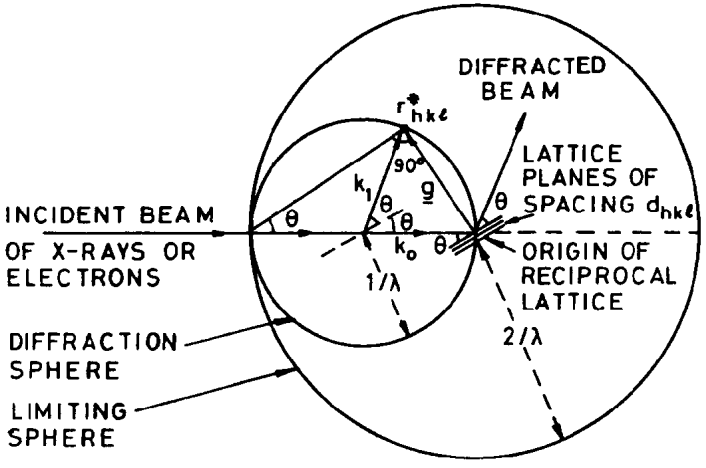

Figure 2.4 Ewald sphere construction for diffraction in the reciprocal lattice.

2.5 Electron Target Interactions

Electron optical imaging and chemical analysis systems are based upon detecting, collecting and processing a range of signals that are produced when an electron beam interacts with either bulk or foil samples. Here we consider the origins and types of interactions which may occur and their use will be described in the following Sections.

Figures 2.5(a) and (b) show beams of high energy electrons interacting with bulk and foil samples respectively. The incident electrons will have energies typically in the range 10 to 100 keV although this could extend up to ~ 1000 keV in the case of foil samples. As the incident electron beam penetrates the bulk sample, Figure 2.5(a), it is slowed, almost continuously, by a large number of inelastic collisions with orbital electrons of the atoms in the crystal lattice (13)(14). In addition, the beam is scattered and spread by a correspondingly large number of elastic interactions with atom nuclei (Rutherford interactions) (15). The penetration of an electron into a solid as a function of incident beam energy is described by its mean free path which is, in turn, a function of beam energy. This is illustrated in Figure 2.6(a) for electrons up to 1000 eV and in Figure 2.6(b) for electrons up to 40 keV. The penetration is also governed by the mass of the atom in the solid and the variation of mean free path with atomic number which is shown in Figure 2.6(c) for an incident beam energy of 30 keV. Only a few of these latter events cause electrons to be deflected through large angles; however, the overall effect of a succession of small angle scattering events is to produce random diffusion in the sample so that electrons towards the end of their trajectories move in directions unrelated to that of the incident beam. The degree of this electron spreading and the depth to which electrons penetrate the sample depends upon incident electron beam voltage, sample material atomic number and density and the angle of tilt of the sample with respect to the incident beam direction. Figure 2.5(a) includes typical values for the depth electron penetration assuming a normal incidence electron probe of 50 keV.

Interaction of an incident electron beam with a bulk sample results in the electrons being either backscattered or emitted as secondary or Auger electrons. Electrons remaining within the sample are eventually absorbed causing it to become charged or they flow to ground as a specimen current. The volume of interaction is typically a 'pear-shape' and it is from within this volume that characteristic X-rays are emitted (16-20). The primary electron beam causes inner shell electrons to either leave the atom entirely as secondary electrons or to be excited to a higher, unoccupied electron orbital. X-ray emission occurs when the resulting electron vacancy is filled by an electron falling from a higher energy level. The X-ray photon has an energy equal to the difference in electron binding energies and a frequency given by $E_1-E_2=h\nu$. Alternatively an Auger electron may be emitted in place of an X-ray photon. In the case following the creation of a vacancy in the inner electron shell the atom may be reorganised by an electron from a higher shell falling into the vacancy and the energy released, (E_1-E_2), is then transferred to an outer shell electron which may be ejected with energy $E = E_1-E_2-E_3$ where E_1,E_2 and E_3 are the electron binding energies, Section 7.4. Since the atoms have a characteristic set of energy levels it follows that there will be a spectrum of Auger emission energies. Auger electron production is most efficient in the range 5 to 1000 eV so that these electrons escape only from the uppermost atomic layer, $\leq$ 5nm, of a sample (21). On the other hand the X-ray photons have a mean free path length which is much greater than that associated with electrons and consequently the depth from which characteristic

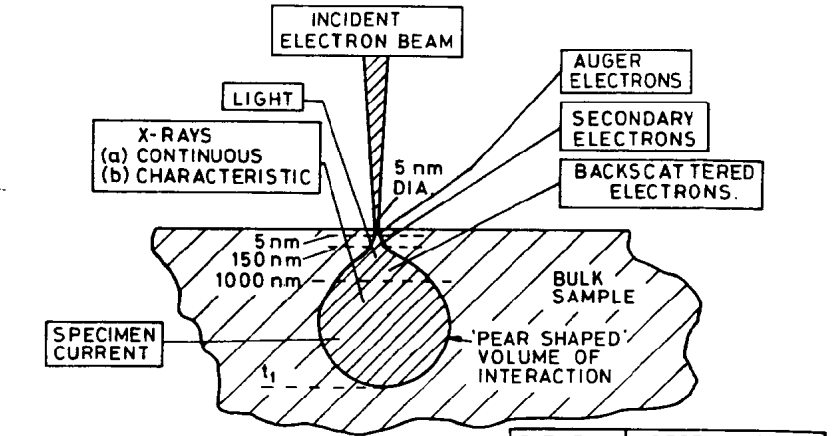

ELEMENT	DEPTH t_1 (μm)
Al	1.5
Cu	0.58
Ag	0.49
Au	0.26

(a)

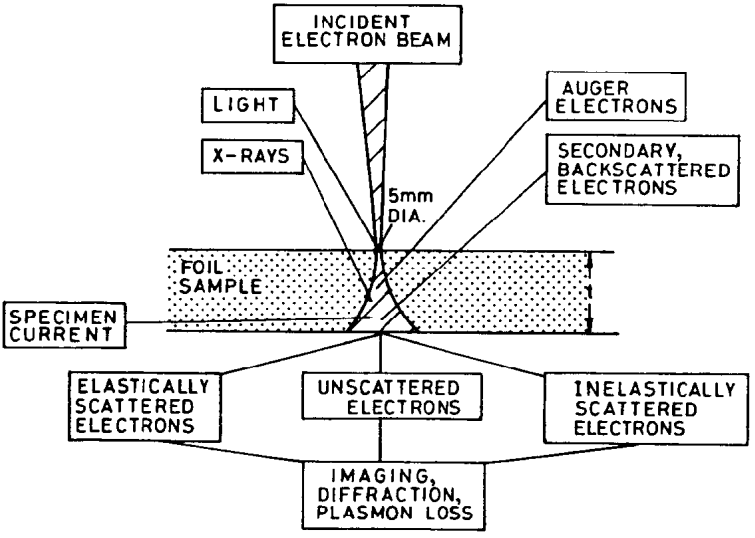

(b)

Figure 2.5 Schematic diagrams showing the interaction of an incident electron beam with:

(a) A bulk specimen showing the 'spread' of the beam and the activated volume giving rise to (i) backscattered, secondary and Auger electrons (ii) characteristic X-rays and (iii) electron current. Typical values given for the depth of electron penetration and the excited volume for a 30 keV, 100nm diameter electron probe.

(b) A foil specimen of thickness, t, ($t \lesssim 300$nm) where in addition to (a) transmitted signals give (i) image contrast and electron diffraction (ii) Kikuchi diffraction and (iii) plasmon losses.